Supplementary Information

Vacuum Nano-Hole Array Embedded Organic Light Emitting Diodes

Sohee Jeon,[a,b] Jun-Ho Jeong,[b] Young Seok Song,[c] Won-Ik Jeong,[a] Jang-Joo Kim[a] and Jae Ryoun Youn*

1. NHA Substrate Fabrication and Characterization

In order to maximize the refractive index contrast of PCs for a given background material, we propose that the low vacuum nanohole array be transferred to the glass substrate in the PC slab using the robust reverse transfer (R^2T) process. **Figure S1a** and **S1b** are SEM images of the NHA substrate and the OLEDs integrated on the NHA substrate. The subsequent layers were evenly deposited on the NHA substrate. On the other hand, the PNA substrate, which

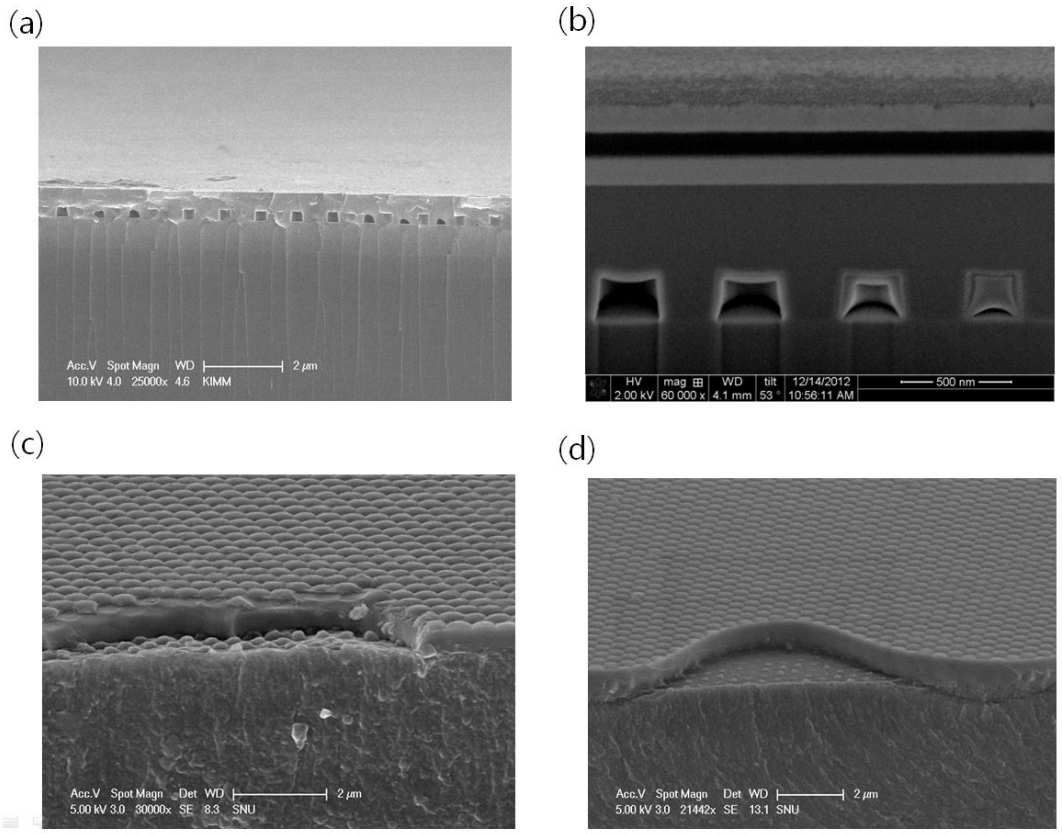

Figure S1. SEM images of (a) the nano-hole array substrate. The trapped low vacuum state was periodically arranged by R^2T process. (b) OLEDs integrated on the NHA substrate. (c) and (d) The Si_3N_4/polymer nanoarray (PNA) substrate. The 500 nm (c) and 800 nm (d) planarized dielectric material (Si_3N_4) deposited using PECVD.

was planarized through plasma enhanced chemical vapor deposition (PECVD) on the polymer array, has a wavy surface and peak points, As a result, the above layers also have wavy and peaky surfaces along the surface of the substrate. The roughness of the substrate has a strong influence on the electrical characteristics of devices.

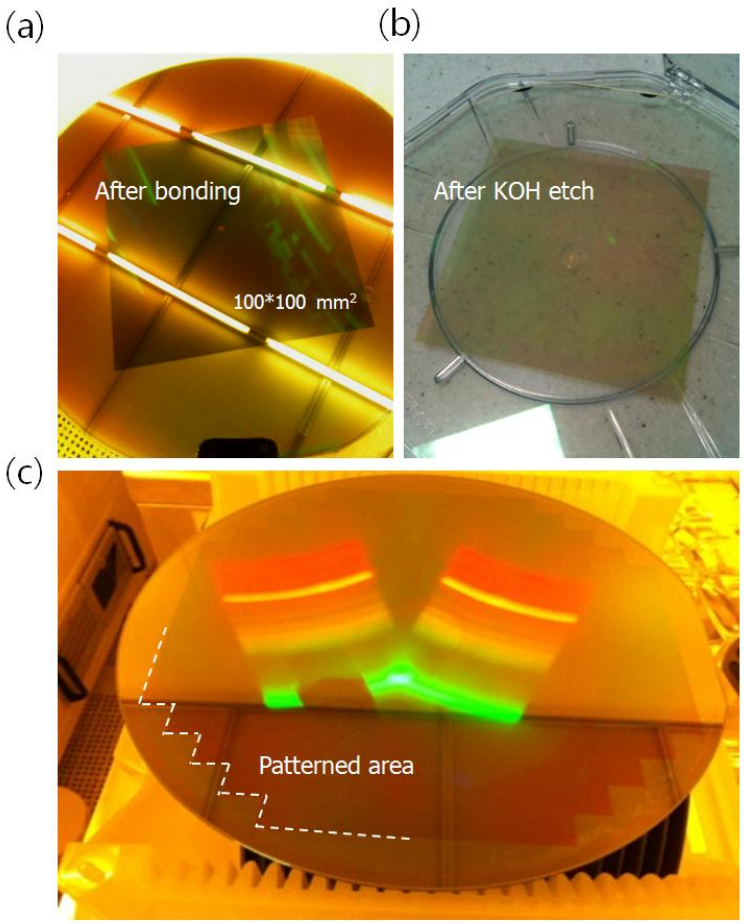

Figure S2. The photographs (a) after anodic bonding, and (b) after removing silicon by dipping KOH solution. The periodic hole is defined over 100*100 mm^2 on 8-inch silicon wafer. and (c) Fully patterned wafer in order to increase the number of samples.

The robust reverse-transfer method was based on the 8-inch wafer process in this study, and then OLEDs devices were fabricated on the substrate diced into 25*25 mm^2. Furthermore, the R^2T bonding is almost a defect-free process over the entire region of an 8-inch wafer as shown in **Figure S2**. Figure S2a shows the wafer after anodic bonding process between the nano-holes patterned Si_3N_4 on silicon wafer and glass wafer, and then dipping KOH solution

the bonded wafer, the final substrate is obtained by removing silicon wafer as shown in figure S2b. In order to increase the number of samples, the wafer is fully patterned by step and repeat photolithograpy as shown in figure S2c.

The AFM images of the NHA substrates are shown in **Figures S3a** and **S3b**. The R_a values were on the order of sub-nano scale, which is the same level as that of the polished Si wafer roughness, as represented in the table below. Meanwhile, the R_a values of the PNA substrate are tens of times larger than those of the NHA substrates, as shown in **Figure S4**. Especially, R_{pv} has a critical effect on the performance of electrical devices, because electric fields are focused on a peaky point, and, as such, a concentrated electric field can permanently damage organic materials. By proposing this R^2T process, we can achieve an NHA substrate that not only has a sub-nano level of roughness to its surface but also maximizes the RI contrast of the PC structure.

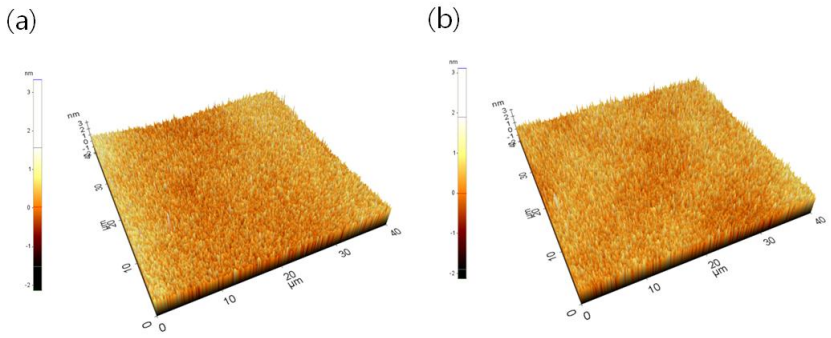

	R_a (nm)	R_{ms} (nm)	R_{pv} (nm)
Specimen 1	0.314	0.401	5.467
Specimen 2	0.341	0.435	5.241
Specimen 3	0.353	0.466	13.459

Figure S3. (a) and (b) AFM images of the NHA substrates. The roughness data of several NHA substrates are summarized in the table below.

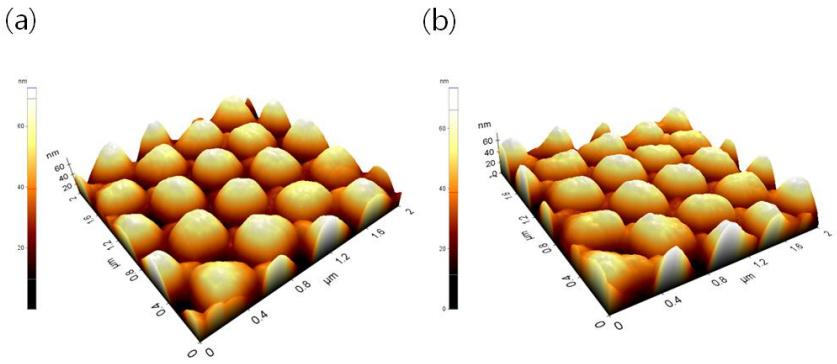

The PNA substrate	R_a (nm)	R_{ms} (nm)	R_{pv} (nm)
Specimen 1	13.398	15.801	57.434
Specimen 2	11.211	13.451	47.381
Specimen 3	12.590	15.138	55.217

Electrode on the PNA substrate	R_a (nm)	R_{ms} (nm)	R_{pv} (nm)
Specimen 1	13.153	15.210	51.057
Specimen 2	10.838	13.492	54.542
Specimen 3	9.476	11.463	43.310

Figure S4. AFM images of (a) the PNA substrates and (b) an electrode surface after sputtering 150 nm-thick ITO layers on the PNA substrates. The roughness data for the PNA substrates and for the electrode on the PNA substrates are summarized in the table below.

2. FDTD simulation

The simulation is performed for a structure identical to the experimental structure. The domain size of the numerical calculation was 8000 × 8000 × 1950 nm^3 which included the actual device: the anode, organic materials, cathode, and corresponding nanostructure layer. Point dipole sources were placed inside of the organic layer at the Alq_3/NPB interface and located at the center of the plane. The wavelength and FWHM (full width at half maximum) were set to be the same as those of PL, 520 nm and 50 nm, respectively. The simulated Poynting energy was detected by the monitor inside the glass and the distance from the dipole source was fixed at the same value. The energy passing though the monitor was obtained by integrating the simulated Poynting energy over time, area, and frequency.

To observe the dependence of the dipole location on the Poynting energy, we estimated the extracting energies that propagated from each dipole at the 16 different positions in the unit cell, and around the unit cell's circumference, as shown in **Figure S5a**. **Figure S5c** and **S5d** show the time integrated Poynting energy according to the polarization of the transverse magnetic (TM) and transverse electric (TE) dipoles at each point: the extracting Poynting energy is the same regardless of the dipole locations. Therefore, we can reduce the calculation time, since it is possible that only one dipole will be sufficient to describe the emission source.

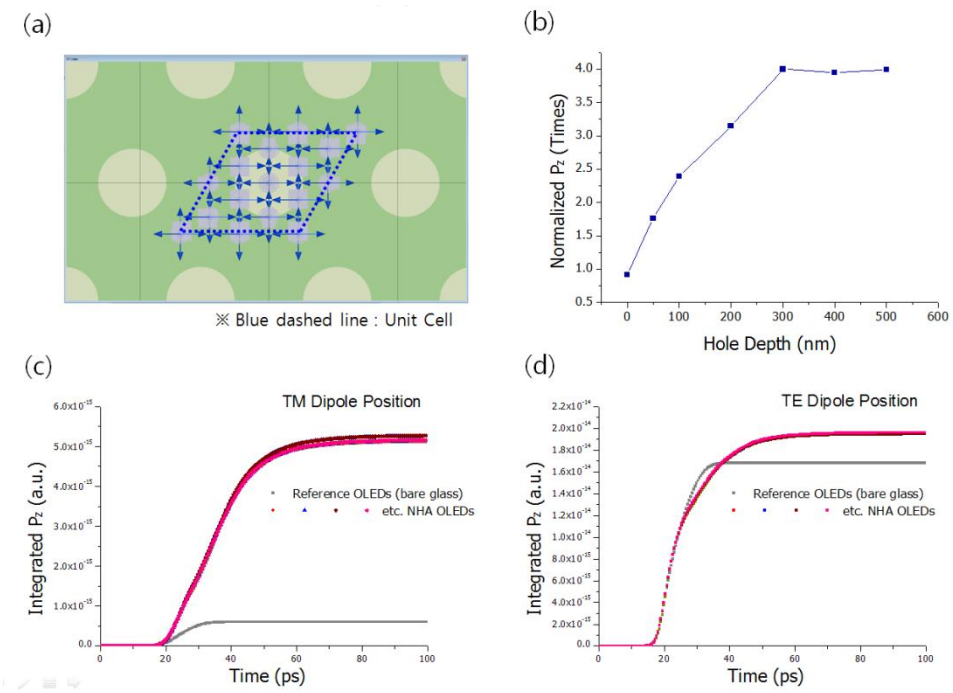

Figure S5. (a) A unit cell of a hexagonal nanostructure. The blue dashed line indicates a unit cell; the 16-different locations are set around the circumference of this cell and inside of it. (b) The Poyinting energy was estimated by varying the hole depth of the nanostructure. The time integrated Poynting energy according to the dipole polarization of TM (c) and TE (d).

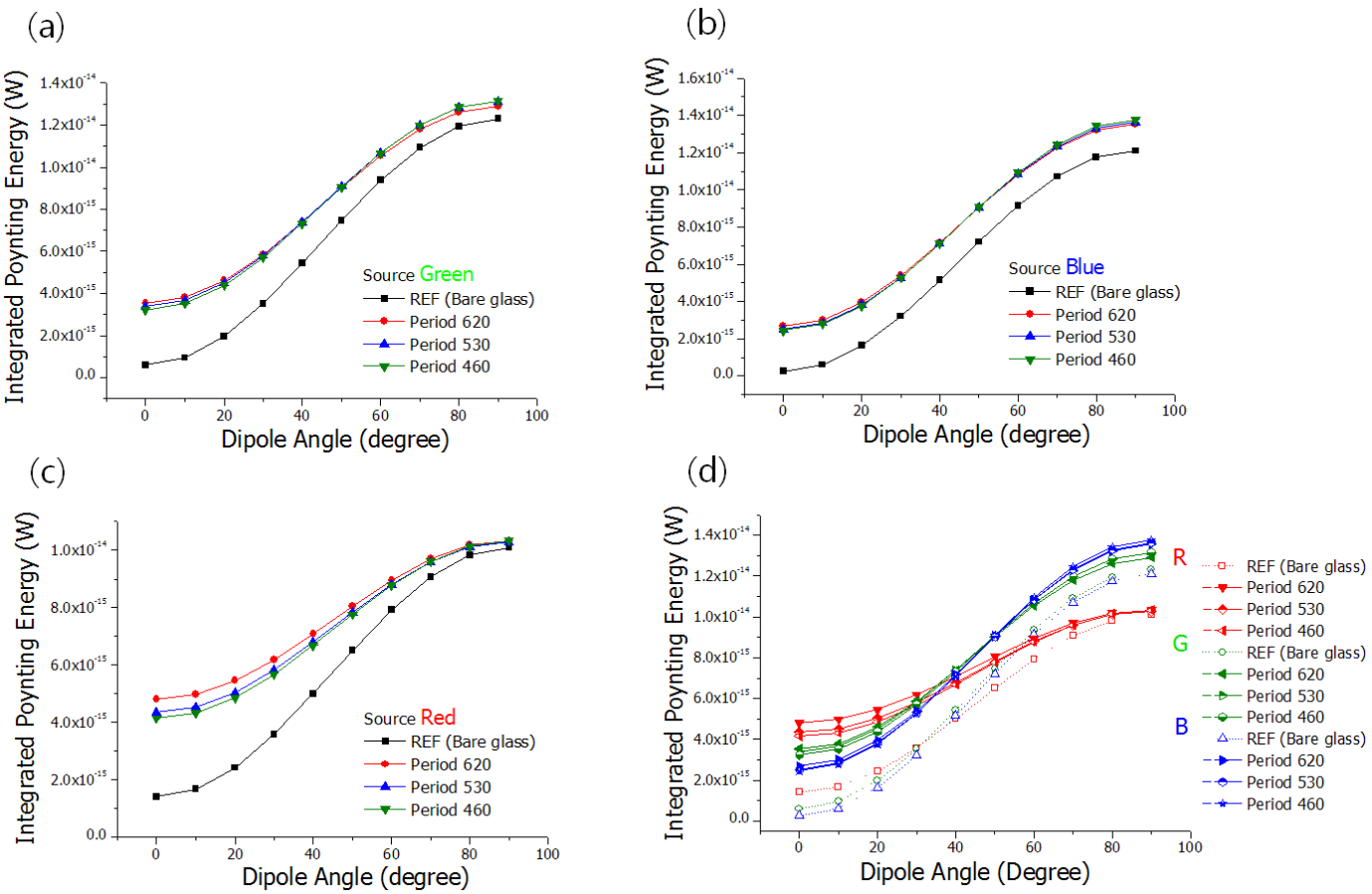

Figure S6. FDTD analysis according to the lattice constants for green (a), blue (b), and red (c); all of the results are shown in one graph (d).

On the other hand, the lattice constant of PC varies from 460 to 620 nm according to visible wavelength range because the extraction efficiency becomes largest when the lattice constant is close to the vacuum wavelength, as discussed in the main text. FDTD simulations were performed by varying dipole angles for various designs of PC structures and colors of light sources according to each combination of the three different lattice constants and the three different wavelengths. As shown in **Figure S6**, the integrated Poynting energies were almost identical regardless of the lattice constant or the wavelength of the dipole sources. As mentioned in the main text, it is confirmed that the crucial factor is the RI difference between n_{low} and n_{high}, rather than the lattice constant of the PCs.

Meanwhile, FDTD simulation was carried out by varying the hole depth of the nanoarray. The Poynting energy as a function of hole depth was saturated until the hole depth reached 300 nm, as shown in **Figure S5b**, so the depth was set at 300 nm.

3. Angular Photoluminescence Characteristics

3.1 Angular PL specimen fabrication

To obtain Angular PL samples, 50nm thick 1% C545T doped Alq_3 was deposited on the NHA and bare substrates (fused silica) by thermal evaporation. The dopant, 1% C545T, was co-evaporated because the PL intensity of Alq_3, induced by 325 laser, was too weak to catch its signal and the dopant just made the PL intensity strong but did not change the dipole orientation.

3.2 Angular PL measurement set-up

Figure S7 shows the angle dependent PL measurement set-up.[1] To measure the angle dependence of PL, the PL specimens were scanned through the ΓM direction corresponding to the constructive plane as the viewing angle was varied with the interval of one degree. A 100 mm diameter fused silica half-cylinder was attached to the PL specimen using index matching oil. The PL emission through the half-cylinder was measured using the photo-detector linked with a monochrometer, chopper, and lock-in amplifier. Those signals were amplified using a photo multiplier tube (PMT). The measurement set-up is illustrated in the **Figure S7** of the supporting information. The linear polarized continuous wave laser diode (λ=325 nm) is used as an optical exciting source. The optical source is injected through the sample tilted at 45° with respect to the substrate surface in order to excite the entire dipoles equally regardless of dipole orientation.

By using index matching oil, the PL sample is attached on a fused silica half cylinder with a diameter of 100 mm. The emission light can directly escape and, due to the spherical surface, does not experience TIR at the interface between the glass and air, so we can easily compare these results to those of the PL experiment and to the FDTD simulation results. A 325 nm wavelength laser source was injected at an angle of 45-degrees to the PL sample surface in order to excite all the dipoles regardless of their orientation. In addition, the source parts of the angle dependent PL measurement set-up were put on a rotation stage, and so the intensities can be measured as a function of the viewing angle. The light is transmitted by a linear polarizer before reaching the detector. The s- and p-polarizers separate the light induced from the d_y dipoles and the d_x/d_z dipoles, respectively.

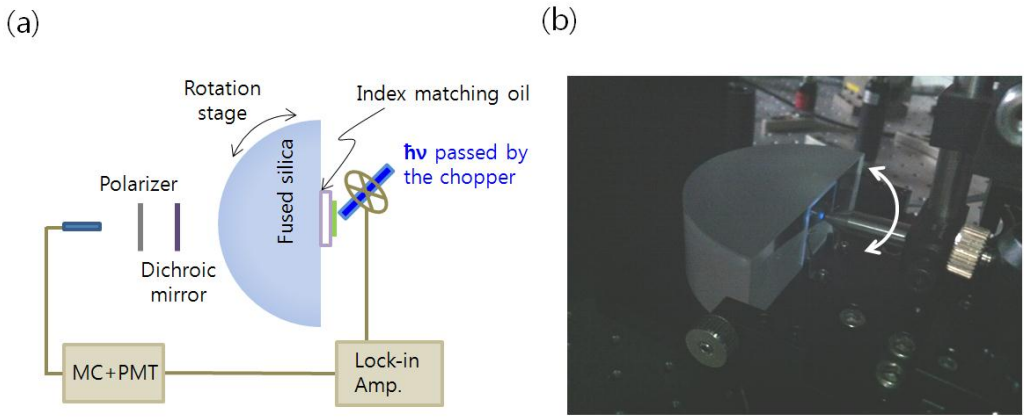

Figure S7. (a) Schematic diagram and (b) photograph of the angle dependent PL measurement set-up.

4. OLED fabrication

OLEDs were fabricated on the NHA and bare substrates. An IZO anode, which was 150 nm thick, was sputtered on the substrate, and the organic and metallic layers were sequentially deposited by thermal evaporation in the following order: a hole injection layer of 60 nm thick 2TNATA (4,4',4''-Tris(N-(2-naphthyl)-N-phenyl-amino)-triphenylamine), a hole transporting

layer of 20 nm thick NPB (N,N'-diphenyl-N,N'-bis(1,1'-biphenyl)-4,4'-diamine), an emitting and electron transporting layer of 60 nm thick Alq_3 (tris-(8-hydroxyquinoline)-aluminum) and a cathode of 1/100 nm thick LiF/Al.

5. EL measurement set-up

The current-voltage characteristics and the light output power of the devices were measured using a source measurement unit (Keithley 237) and a photodiode (Newport Model 818-UV) connected to an optical power meter (Newport Model 1835-C). Electroluminescence intensity of each sample was measured using an integrating sphere (Labsphere Co., 6" diameter) in order to detect all the light emitted in the forward direction from the device. The device was attached to a port of the integrating sphere where the glass side was facing toward the inside of the integrating sphere. The angle dependence of the EL intensity was measured by a photo-spectrometer (PR650) in every 5 degrees of the viewing angle.

6. Effects of Si_3N_4 buffer layer thickness on the light extraction

The thickness of the buffer layer (Si_3N_4, the distance between IZO and the NHA, *d*) is determined empirically using PL and EL measurement with 8-inch integrating sphere. The light trapped in the IZO and organic layer can propagate to the Si_3N_4 (used as a high index material, n_{Si3N4}=2.02 at the wavelength of 520 nm) without experiencing the total internal reflection at the IZO and Si_3N_4 interface, because the refractive indices of organic layer and IZO are smaller than that of Si_3N_4 (n_{org}=1.7 and n_{IZO}=1.98[2]). Accordingly, once the light propagated to the high index layer (Si_3N_4) and then interacted with the NHA and finally got a chance to escape to the air. The performance of the NHA OLED having different thickness of the buffer layer was estimated by photoluminescence (PL) measurement, and the distance

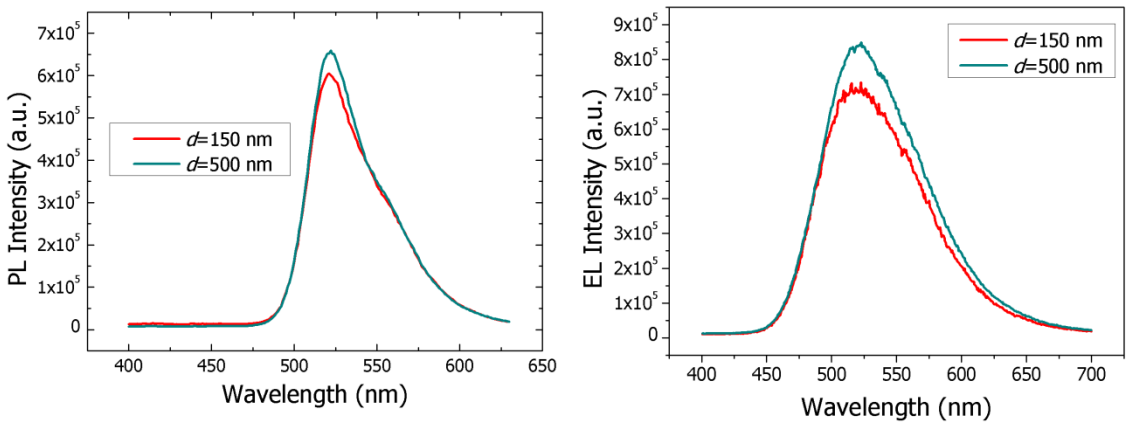

Figure S8. The light extraction performance was estimated by varying the thickness of the buffer layer. The PL and EL intensities were measured using an 8-inch integrating sphere. The buffer layers (the distance between IZO and the NHA, *d*) are 150 nm and 500 nm.

between IZO and the NHA (*d*) was 150 and 500 nm. As shown in the figure S8, both of the PL and EL intensities are larger in the case of *d*=500nm, rather than that of *d*=150 nm. Moreover, the buffer layer should be thick enough for the device fabrication. Because the thickness (*d*) is too thin, the film can be broken in an extremely high vacuum state (~10^{-7} Torr) during the device fabrication.

Notes and references

[a]Research Institute of Advanced Materials (RIAM), Department of Materials Science and Engineering, Seoul National University, Seoul, 151-744, Korea

[b]Nano-Mechanical Systems Research Center, Korea Institute of Machinery and Materials, Daejeon, 305-343, Korea

[c]Department of Fiber System Engineering, Dankook University, Yongin, Gyeonggi, 448-701, Korea

1. J. Frischeisen, D. Yokoyama, C. Adachi and W. Brutting, *Appl. Phys. Lett.*, 2010, **96**.

2. S. T. Kim, J. H. Lee, J. Y. Yang, S. W. Ryu, J. S. Hong, W. P. Hong, J. J. Kim, H. M. Kim, J. M. Yang and S. H. Park, *J. Korean Phys. Soc.*, 2007, **50**, 662-665